PETSC TSADJOINT: A DISCRETE ADJOINT ODE SOLVER FOR FIRST-ORDER AND SECOND-ORDER SENSITIVITY ANALYSIS [*]

HONG ZHANG[†], EMIL M. CONSTANTINESCU[‡], AND BARRY F. SMITH[§]

Abstract. We present a new software system `PETSc TSAdjoint` for first-order and second-order adjoint sensitivity analysis of time-dependent nonlinear differential equations. The derivative calculation in `PETSc TSAdjoint` is essentially a high-level algorithmic differentiation process. The adjoint models are derived by differentiating the timestepping algorithms and implemented based on the parallel infrastructure in `PETSc`. Full differentiation of the library code including MPI routines thus is avoided, and users do not need to derive their own adjoint models for their specific applications. `PETSc TSAdjoint` can compute the first-order derivative, that is, the gradient of a scalar functional, and the Hessian-vector product that carries second-order derivative information, while requiring minimal input (a few callbacks) from the users. Optimal checkpointing schemes are employed by the adjoint model in a manner that is transparent to users. Usability, efficiency, and scalability are demonstrated through examples from a variety of applications.

Key words. sensitivity analysis, adjoint, PETSc, second-order adjoint

AMS subject classifications. 97N80, 65L99, 49Q12

1. Introduction.

Adjoint methods have been used extensively in computational modeling and optimization, playing a key role in neural networks, sensitivity analysis, goal-oriented error estimation, data assimilation, and optimal control. They are efficient Algorithmic Differentiation (AD) approaches for computing the derivatives of an objective function of the solution of an ordinary differential equation (ODE) or differential-algebraic equation (DAE), with respect to parameters of interest, with a cost independent of the number of parameters. Deriving the adjoint model is trivial for linear models, but can be difficult for nonlinear models [12], especially time-dependent problems.

Many tools have been developed to automatically derive and implement adjoint models. These automatic tools take as input a forward model that users implement in languages such as C [6, 32], C++ [24], Fortran [14], Python [23] and Julia [21], and produce as output the associated discrete adjoint model in a line-by-line fashion, through source-to-source transformations, operator overloading or a combination of both. While this black-box approach gives the highest degree of automation and requires the least knowledge of the mathematical models, it suffers from many low-level implementation-specific difficulties including memory allocation, management of pointers, input/output, and parallel communication (e.g. MPI and OpenMP). Such black box tools also often produce far from optimally efficient code.

Traditional AD treats a model as a sequence of primitive instructions (e.g., addition, multiplication, logarithm), and calculates the derivatives based on the chain rule using the derivatives of these primitive instructions, which are easily obtainable. To overcome the low-level difficulties, recently, high-level AD libraries such as `dolfin-adjoint` [12], `FATODE` [36], have been developed to operate at high abstraction

[*]Submitted to the editors DATE.

Funding: This material is based upon work supported by the U.S. Department of Energy, Office of Science, Office of Advanced Scientific Computing Research, Scientific Discovery through Advanced Computing (SciDAC) program through the FASTMath Institute under contract DE-AC02-06CH11357 at Argonne National Labortory.

[†]Argonne National Laboratory, Lemont, IL (hongzhang@anl.gov).
[‡]Argonne National Laboratory, Lemont, IL (emconsta@anl.gov).
[§]Argonne National Laboratory, Lemont, IL (bsmith@mcs.anl.gov).

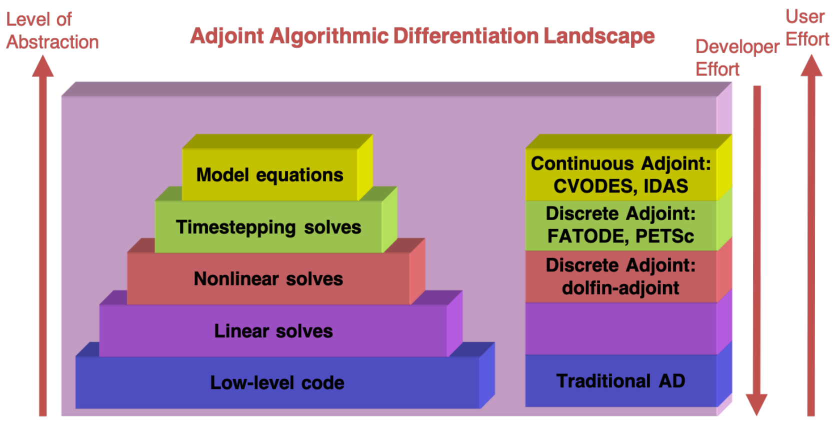
Level of Abstraction
Adjoint Algorithmic Differentiation Landscape
Developer Effort
User Effort
Model equations
Timestepping solves
Nonlinear solves
Linear solves
Low-level code
Continuous Adjoint: CVODES, IDAS
Discrete Adjoint: FATODE, PETSc
Discrete Adjoint: dolfin-adjoint
Traditional AD

Fig. 1: Landscape of adjoint algorithmic differetiation software.

levels.

The landscape of popular existing AD software is depicted in Fig. 1. While these software packages are developed based on the same theory, they differ significantly in usage and require varying levels of effort from developers' and users' perspectives. `dolfin-adjoint` [12] considers a model as a sequence of nonlinear equation solves. The derivation of the adjoint model is fully automated in `dolfin-adjoint` if the forward model is written in a high-level language that is similar to mathematical notation. `dolfin-adjoint` is primaritly used by finite element system such as `FEniCS` [3] and `Firedrake` [26]. `FATODE` implements an adjoint model by considering the algorithm of solving time-dependent differential equations as a sequence of timestepping solves. `FATODE` provides a built-in implementation of the adjoint model derived based on the timestepping algorithms for solving ordinary differential equations (ODEs); simulation of time-dependent partial differential equations (PDEs) is abstracted as a sequence of time steps, and the libraries differentiate each time step. In contrast, the adjoint solvers `CVODES` and `IDAS` in the `SUNDIALS` [17] package implement an adjoint model that users derive directly from the model equations. This highest-level approach is also known as the continuous adjoint approach, which requires users to derive a new set of equations before discretization (adjoint model of the original continuum or weak form mode). All the other aforementioned approaches are discrete adjoint approaches since the adjoint models are derived after discretization. In general, lower-level abstractions tend to impose more implementation burden on library developers and provide more automation to users and, at the same time, hide more mathematical structures from users.

Adopting the similar approach used by `FATODE`, we have over the past few years developed the `TSAdjoint` component in the Portable, Extensible Toolkit for Scientific Computation `PETSc` [1, 34]. `PETSc` `TSAdjoint` enables first- and second-order adjoint sensitivity analysis for nonlinear time-dependent differential equations that is the key ingredient of many gradient-based optimization algorithms. The adjoint models are derived and implemented for various time integrators in `PETSc`. As a result, the adjoint models employ the parallel infrastructure and the sophisticated linear/nonlinear solvers in `PETSc` in the same way as the forward models do. Optimal adjoint checkpoiting schemes are implemented, and the adjoint control flow is managed automatically by `PETSc`. These features are significant advantages in achieving the efficiency of adjoint calculation compared with other adjoint codes.

In the next section we provide the mathematical foundations of sensitivity analysis for ODE integrators. In Section 3 we explain the software infrastructure. Section 4 discusses the management of the required checkpointing and Section 5 explores the use of these algorithms in four examples.

2. Mathematical Foundation.

In this section, we explain how the sensitivity propagation equations are derived based on the model abstraction at the timestepping level. Both first-order and second-order sensitivity analysis approaches are covered. An example using theta timestepping methods for which the adjoint model has moderate complexity, is given to illustrate the details of the derivation. The mathematical framework can be naturally extended to other timestepping algorithms including explicit schemes and even implicit-explicit schemes.

The goal of sensitivity analysis of a dynamical system is to compute the derivative of a scalar functional with respect to certain system parameters. For notational brevity and without loss of generality, we consider the dynamical system in differential-algebraic equation (DAE) form

$$\boldsymbol{\mathcal{M}}\dot{\boldsymbol{u}} = \boldsymbol{f}(t, \boldsymbol{u}; \boldsymbol{p}) \tag{2.1}$$

where $\boldsymbol{\mathcal{M}} \in \mathbb{R}^{N_d \times N_d}$ is the mass matrix, $\boldsymbol{u} \in \mathbb{R}^{N_d}$ is the system state and $\boldsymbol{p} \in \mathbb{R}^{N_p}$ is the parameters of interest. These forms typically arise from semi-discretization of time-dependent PDEs using the method of lines. The mass matrix may be the identity for typical ODEs or a singular matrix for DAEs. In this paper, vectors and matrices are denoted by bold letters and scalars by non-bold letters. The *numerator layout* notation is used for derivatives; for example, the gradient of a scalar function is a row vector.

Consider time integration as a sequence of operations

$$\boldsymbol{u}_{n+1} = \boldsymbol{\mathcal{N}}(\boldsymbol{u}_n), \quad n = 0, \ldots, N-1, \tag{2.2}$$

where the initial condition is $\boldsymbol{u}_0 = \boldsymbol{\eta}$ and $\boldsymbol{\mathcal{N}}$ is a timestepping operator that propagates the solution from t_n to t_{n+1}. As an example of $\boldsymbol{\mathcal{N}}$, an implicit timestepping method is discussed in Section 2.3. The scalar functional in sensitivity analysis depends on the system states and is denoted by $\psi(\boldsymbol{u}_N)$ if it is a function of the final state or expressed in integral form

$$\int_{t_0}^{t_F} r(t, \boldsymbol{u}; \boldsymbol{p}) dt \tag{2.3}$$

if it is a function of the entire trajectory of the system.

In the following two subsections, we briefly explain how the derivatives of a scalar function $\psi(\boldsymbol{u}_N)$ with respect to the initial condition are derived in the discrete regime. The derivatives with respect to parameters (e.g., model parameters) can be derived with the same framework by augmenting the parameters into the initial condition vector. We refer readers to [36] for details.

2.1. First-order discrete derivatives.

We use the Lagrange multipliers $\boldsymbol{\lambda}_n \in \mathbb{R}^{N_d}, n = 0, \ldots, N$, which are column vectors, to account for the constraint from each time step, and we define the Lagrangian

$$\mathcal{L}(\boldsymbol{\eta}) = \psi(\boldsymbol{u}_N) - \boldsymbol{\lambda}_0^T (\boldsymbol{u}_0 - \boldsymbol{\eta}) - \sum_{n=0}^{N-1} \boldsymbol{\lambda}_{n+1}^T (\boldsymbol{u}_{n+1} - \boldsymbol{\mathcal{N}}(\boldsymbol{u}_n)) . \tag{2.4}$$

We choose the transpose for the convenience of derivation because the derivative of a row vector with respect to a column vector is not well defined in matrix calculus.

Differentiating equation (2.4) with respect to the initial condition $\boldsymbol{\eta}$ leads to

$$\frac{d\mathcal{L}}{d\boldsymbol{\eta}} = \boldsymbol{\lambda}_0^T - \left(\frac{d\psi}{d\boldsymbol{u}}(\boldsymbol{u}_N) - \boldsymbol{\lambda}_N^T\right) \frac{\partial \boldsymbol{u}_N}{\partial \boldsymbol{\eta}} - \sum_{n=0}^{N-1} \left(\boldsymbol{\lambda}_n^T - \boldsymbol{\lambda}_{n+1}^T \frac{d\boldsymbol{\mathcal{N}}}{d\boldsymbol{u}}(\boldsymbol{u}_n)\right) \frac{\partial \boldsymbol{u}_n}{\partial \boldsymbol{\eta}} . \tag{2.5}$$

The first-order adjoint equation is defined as

$$\begin{aligned} \boldsymbol{\lambda}_n &= \left(\frac{d\boldsymbol{\mathcal{N}}}{d\boldsymbol{u}}(\boldsymbol{u}_n)\right)^T \boldsymbol{\lambda}_{n+1}, \quad n = N-1, \ldots, 0, \\ \boldsymbol{\lambda}_N &= \left(\frac{d\psi}{d\boldsymbol{u}}(\boldsymbol{u}_N)\right)^T , \end{aligned} \tag{2.6}$$

in order to make the last two terms in (2.5) vanish. Note that in the adjoint model the sensitivities are calculated by propagating the derivative information in reverse order.

An alternative approach is to derive the discrete tangent linear model (TLM) from the discrete forward model. By differentiating directly (2.2) with respect to the initial condition $\boldsymbol{\eta}$ and defining the sensitivity matrix $\boldsymbol{\mathcal{S}}_n \in \mathbb{R}^{N_d \times N_d}$ by

$$\boldsymbol{\mathcal{S}}_n = \frac{d\boldsymbol{u}_n}{d\boldsymbol{\eta}}, \quad n = 0, \ldots, N-1, \tag{2.7}$$

we can obtain the TLM equations

$$\boldsymbol{\mathcal{S}}_{n+1} = \left(\frac{d\boldsymbol{\mathcal{N}}}{d\boldsymbol{u}}(\boldsymbol{u}_n)\right) \boldsymbol{\mathcal{S}}_n, \quad n = 0, \ldots, N-1, \tag{2.8}$$

which propagates the sensitivity matrix forward in time and can be solved together with the original model equations (2.1). Similarly, one can differentiate (2.2) with respect to parameters in order to derive the TLM for calculating parameter sensitivities. These sensitivities can be used to compute the derivative of the scalar functional through the chain rule, so that the TLM method can achieve the same goal as the adjoint method. However, these two methods may differ significantly in terms of computational cost. The adjoint method is known to be efficient when computing derivatives of a scalar functional with respect to a large number of parameters. The TLM method can be efficient only when there are few parameters and thus has limited application compared with the adjoint method.

2.2. Second-order discrete derivatives. The most efficient approach for calculating second-order derivatives is the forward-over-adjoint method [2], which requires both the first adjoint model and the TLM. By differentiating the transpose of

$\frac{d\mathcal{L}}{d\boldsymbol{\eta}}$ with respect to $\boldsymbol{\eta}$ for a second time, we obtain

(2.9)
$$\begin{aligned}\frac{d}{d\boldsymbol{\eta}}\left(\frac{d\mathcal{L}}{d\boldsymbol{\eta}}\right)^T &= \frac{d\boldsymbol{\lambda}_0}{d\boldsymbol{\eta}} - \left(\frac{d\psi}{d\boldsymbol{u}}(\boldsymbol{u}_N) - \boldsymbol{\lambda}_N^T\right)\frac{\partial^2 \boldsymbol{u}_N}{\partial \boldsymbol{\eta}^2} \\ &- \left(\frac{\partial \boldsymbol{u}_N}{\partial \boldsymbol{\eta}}\right)^T\left(\frac{d}{d\boldsymbol{u}}\left(\frac{d\psi}{d\boldsymbol{u}}(\boldsymbol{u}_N)\right)^T \frac{\partial \boldsymbol{u}_N}{\partial \boldsymbol{\eta}} - \frac{d\boldsymbol{\lambda}_N}{d\boldsymbol{\eta}}\right) \\ &- \sum_{n=0}^{N-1}\left(\frac{\partial \boldsymbol{u}_n}{\partial \boldsymbol{\eta}}\right)^T\left(\frac{d\boldsymbol{\lambda}_n}{d\boldsymbol{\eta}} - \boldsymbol{\lambda}_{n+1}^T\frac{d^2\boldsymbol{\mathcal{N}}}{d\boldsymbol{u}^2}(\boldsymbol{u}_n)\frac{\partial \boldsymbol{u}_n}{\partial \boldsymbol{\eta}} - \left(\frac{d\boldsymbol{\mathcal{N}}}{d\boldsymbol{u}}(\boldsymbol{u}_n)\right)^T\frac{d\boldsymbol{\lambda}_n}{d\boldsymbol{\eta}}\right) \\ &- \sum_{n=0}^{N-1}\left(\boldsymbol{\lambda}_n^T - \left(\frac{d\boldsymbol{\mathcal{N}}}{d\boldsymbol{u}}(\boldsymbol{u}_n)\right)^T\boldsymbol{\lambda}_{n+1}\right)\frac{\partial^2 \boldsymbol{u}_n}{\partial \boldsymbol{\eta}^2}.\end{aligned}$$

By utilizing the first-order adjoint equations (2.6) and the second-order adjoint equations

$$\begin{aligned}\frac{d\boldsymbol{\lambda}_n}{d\boldsymbol{\eta}} &= \left(\frac{d\boldsymbol{\mathcal{N}}}{d\boldsymbol{u}}(\boldsymbol{u}_n)\right)^T\frac{d\boldsymbol{\lambda}_{n+1}}{d\boldsymbol{\eta}} + \boldsymbol{\lambda}_{n+1}^T\frac{d^2\boldsymbol{\mathcal{N}}}{d\boldsymbol{u}^2}(\boldsymbol{u}_n)\frac{\partial \boldsymbol{u}_n}{\partial \boldsymbol{\eta}},\ n = N-1,\dots,0, \\ \frac{d\boldsymbol{\lambda}_N}{d\boldsymbol{\eta}} &= \frac{d}{d\boldsymbol{u}}\left(\frac{d\psi}{d\boldsymbol{u}}(\boldsymbol{u}_N)\right)^T\frac{\partial \boldsymbol{u}_N}{\partial \boldsymbol{\eta}},\end{aligned} \tag{2.10}$$

where $\frac{d\boldsymbol{\lambda}}{d\boldsymbol{\eta}}$ carries second-order derivative information, we can obtain the Hessian of the objective function $\nabla^2_{\boldsymbol{\eta}}\mathcal{L} = \nabla^2_{\boldsymbol{\eta}}\psi(\boldsymbol{u}_n) = \frac{d\boldsymbol{\lambda}_0}{d\boldsymbol{\eta}}$ from the solution of these adjoint equations.

Equation (2.10) propagates a matrix, a process that is computationally expensive and is not storage efficient. Practical implementations seek to provide the computation of Hessian-vector products instead of the full Hessian. To this end, we derive the directional second-order derivative instead, which results in a significantly lower complexity. Assume $\boldsymbol{v} \in \mathbb{R}^{N_d}$ is the directional vector that either comes from the optimization algorithm or is specified by the user. Post multipying v from both sides of (2.10) gives

$$\begin{aligned}\frac{d\boldsymbol{\lambda}_n}{d\boldsymbol{\eta}}\boldsymbol{v} &= \left(\frac{d\boldsymbol{\mathcal{N}}}{d\boldsymbol{u}}(\boldsymbol{u}_n)\right)^T\frac{d\boldsymbol{\lambda}_{n+1}}{d\boldsymbol{\eta}}\boldsymbol{v} + \boldsymbol{\lambda}_{n+1}^T\frac{d^2\boldsymbol{\mathcal{N}}}{d\boldsymbol{u}^2}(\boldsymbol{u}_n)\boxed{\frac{\partial \boldsymbol{u}_n}{\partial \boldsymbol{\eta}}\boldsymbol{v}},\ n = N-1,\dots,0, \\ \frac{d\boldsymbol{\lambda}_N}{d\boldsymbol{\eta}}\boldsymbol{v} &= \frac{d}{d\boldsymbol{\eta}}\left(\frac{d\psi}{d\boldsymbol{u}}(\boldsymbol{u}_N)\right)^T\boxed{\frac{\partial \boldsymbol{u}_N}{\partial \boldsymbol{\eta}}\boldsymbol{v}}.\end{aligned} \tag{2.11}$$

The boxed terms in (2.11) are the directional derivatives for the forward sensitivities that can be calculated with a TLM.

These equations can also be derived by differentiating the first-order adjoint equation (2.6). For brevity, we drop $n = N-1,\dots,0$ in the adjoint equations in what follows. Readers should keep in mind that the adjoint equations always go backward in time. Parameters $\boldsymbol{p}$ in functions such as $\boldsymbol{f}$ and r are dropped for the same reason.

2.3. Example: theta methods. As an illustrative example, we describe how the TLM and the first-order and second-order adjoint models are derived for theta methods, which can be written as

$$\boldsymbol{\mathcal{M}}\boldsymbol{u}_{n+1} = \boldsymbol{\mathcal{M}}\boldsymbol{u}_n + h_n(1-\theta)\boldsymbol{f}(\boldsymbol{u}_n) + h_n\theta\boldsymbol{f}(\boldsymbol{u}_{n+1}), \tag{2.12}$$

where $h_n = t_{n+1} - t_n$.

2.3.1. First-order adjoint sensitivity. In its simplest form, the adjoint theta method is

$$\boldsymbol{\mathcal{M}}^T \boldsymbol{\lambda}_s = \boldsymbol{\lambda}_{n+1} + h_n\theta\, \boldsymbol{f}_{\boldsymbol{u}}^T(\boldsymbol{u}_{n+1})\boldsymbol{\lambda}_s \tag{2.13a}$$

$$\boldsymbol{\lambda}_n = \boldsymbol{\mathcal{M}}^T \boldsymbol{\lambda}_s + h_n(1-\theta)\boldsymbol{f}_{\boldsymbol{u}}^T(\boldsymbol{u}_n)\boldsymbol{\lambda}_s. \tag{2.13b}$$

with the terminal condition

$$\boldsymbol{\lambda}_N = \left(\frac{\partial\psi}{\partial\boldsymbol{u}}(\boldsymbol{u}_n)\right)^T. \tag{2.14}$$

By augmenting the state vector with the parameters and the integrand in the objective function (2.3), we obtain a larger system that can be written as

$$\begin{aligned}
\boldsymbol{\mathcal{M}}^T \boldsymbol{\lambda}_s &= \boldsymbol{\lambda}_{n+1} + h_n\theta\, \boldsymbol{f}_{\boldsymbol{u}}^T(\boldsymbol{u}_{n+1})\boldsymbol{\lambda}_s + h_n\theta\, r_{\boldsymbol{u}}^T(t_{n+1},\boldsymbol{u}_{n+1}),\\
\boldsymbol{\lambda}_n &= \boldsymbol{\mathcal{M}}^T \boldsymbol{\lambda}_s + h_n(1-\theta)\boldsymbol{f}_{\boldsymbol{u}}^T(\boldsymbol{u}_n)\boldsymbol{\lambda}_s + h_n(1-\theta)r_{\boldsymbol{u}}^T(t_n,\boldsymbol{u}_n),\\
\boldsymbol{\mu}_n &= \boldsymbol{\mu}_{n+1} + h_n\theta\left(\boldsymbol{f}_{\boldsymbol{p}}^T(\boldsymbol{u}_{n+1})\boldsymbol{\lambda}_s + r_p^T(\boldsymbol{u}_{n+1})\right) + h_n(1-\theta)\left(\boldsymbol{f}_{\boldsymbol{p}}^T(\boldsymbol{u}_n)\boldsymbol{\lambda}_s + r_{\boldsymbol{p}}^T(\boldsymbol{u}_n)\right),
\end{aligned} \tag{2.15}$$

where $\boldsymbol{\mu}_n = \frac{\partial\psi}{\partial\boldsymbol{p}}(\boldsymbol{u}_n)$, $\mathbf{f}_{\{\boldsymbol{u},\boldsymbol{p}\}} = \frac{\partial\mathbf{f}}{\partial\{\boldsymbol{u},\boldsymbol{p}\}}$ and $r_{\{\boldsymbol{u},\boldsymbol{p}\}} = \frac{\partial r}{\partial\{\boldsymbol{u},\boldsymbol{p}\}}$. The corresponding terminal conditions are

$$\boldsymbol{\lambda}_N = \left(\frac{\partial\psi}{\partial\boldsymbol{u}}(\boldsymbol{u}_n)\right)^T, \quad \boldsymbol{\mu}_N = \left(\frac{\partial\psi}{\partial\boldsymbol{p}}(\boldsymbol{u}_n)\right)^T. \tag{2.16}$$

2.3.2. First-order forward sensitivity. We take the derivative of the one-step time integration algorithm (2.12) with respect to parameters $\boldsymbol{p} \in \mathbb{R}^{N_p}$ and obtain the discrete TLM

$$\begin{aligned}
\boldsymbol{\mathcal{M}}\boldsymbol{\mathcal{S}}_{n+1} = \boldsymbol{\mathcal{M}}\boldsymbol{\mathcal{S}}_n + h_n\big((1-\theta)\left(\boldsymbol{f}_{\boldsymbol{u}}(\boldsymbol{u}_n)\boldsymbol{\mathcal{S}}_n + \boldsymbol{f}_{\boldsymbol{p}}(\boldsymbol{u}_n)\right)\\
+ \theta\left(\boldsymbol{f}_{\boldsymbol{u}}(\boldsymbol{u}_{n+1})\boldsymbol{\mathcal{S}}_{n+1} + \boldsymbol{f}_{\boldsymbol{p}}(\boldsymbol{u}_{n+1})\right)\big),
\end{aligned} \tag{2.17}$$

where $\boldsymbol{\mathcal{S}}_n = d\boldsymbol{u}_n/d\boldsymbol{p}$ denotes the solution sensitivities (a.k.a. trajectory sensitivities).

With the solution sensitivities, the total derivative of $\psi(\boldsymbol{u}_n)$ can be computed by using

$$\frac{d\psi}{d\boldsymbol{p}}(\boldsymbol{u}_n) = \frac{\partial\psi}{\partial\boldsymbol{u}}(\boldsymbol{u}_n)\boldsymbol{\mathcal{S}}_N + \frac{\partial\psi}{\partial\boldsymbol{p}}(\boldsymbol{u}_n) \tag{2.18}$$

or in column-vector form

$$\left(\frac{d\psi}{d\boldsymbol{p}}(\boldsymbol{u}_n)\right)^T = \boldsymbol{\mathcal{S}}_N^T\left(\frac{\partial\psi}{\partial\boldsymbol{u}}(\boldsymbol{u}_n)\right)^T + \left(\frac{\partial\psi}{\partial\boldsymbol{p}}(\boldsymbol{u}_n)\right)^T. \tag{2.19}$$

Sensitivity for the integral representation of the objective function is given by

$$\frac{dq}{d\boldsymbol{p}} = \int_{t_0}^{t_F}\left(\frac{\partial r}{\partial\boldsymbol{u}}(\boldsymbol{u})\boldsymbol{\mathcal{S}} + \frac{\partial r}{\partial\boldsymbol{p}}(\boldsymbol{u})\right)dt. \tag{2.20}$$

2.3.3. Second-order adjoint: sensitivities to initial condition. Differentiating the first-order adjoint (2.13) with respect to the initial condition leads to

$$\boldsymbol{\mathcal{M}}^T \frac{d\boldsymbol{\lambda}_s}{d\boldsymbol{\eta}} = \frac{d\boldsymbol{\lambda}_{n+1}}{d\boldsymbol{\eta}} + h_n\theta\boldsymbol{\lambda}_s^T \boldsymbol{f}_{\boldsymbol{uu}}(\boldsymbol{u}_{n+1})\, \frac{d\boldsymbol{u}_{n+1}}{d\boldsymbol{\eta}} + h_n\theta \boldsymbol{f}_{\boldsymbol{u}}^T(\boldsymbol{u}_{n+1})\, \frac{d\boldsymbol{\lambda}_s}{d\boldsymbol{\eta}} \tag{2.21a}$$

$$\frac{d\boldsymbol{\lambda}_n}{d\boldsymbol{\eta}} = \boldsymbol{\mathcal{M}}^T \frac{d\boldsymbol{\lambda}_s}{d\boldsymbol{\eta}} + h_n(1-\theta)\boldsymbol{\lambda}_s^T \boldsymbol{f}_{\boldsymbol{uu}}(\boldsymbol{u}_n)\, \frac{d\boldsymbol{u}_n}{d\boldsymbol{\eta}} + h_n(1-\theta)\boldsymbol{f}_{\boldsymbol{u}}^T(\boldsymbol{u}_n)\, \frac{d\boldsymbol{\lambda}_s}{d\boldsymbol{\eta}}, \tag{2.21b}$$

with the terminal condition

$$\frac{d\boldsymbol{\lambda}_N}{d\boldsymbol{\eta}} = \frac{d}{d\boldsymbol{u}}\left(\frac{d\psi}{d\boldsymbol{u}}(\boldsymbol{u}_n)\right)^T \frac{\partial \boldsymbol{u}_n}{\partial \boldsymbol{\eta}}. \tag{2.22}$$

Post multiplying both sides of (2.21) by a direction vector $\boldsymbol{v} \in \mathbb{R}^{N_d}$ and defining $\boldsymbol{\Lambda} = (d\boldsymbol{\lambda}/d\boldsymbol{\eta})\boldsymbol{v}$ to shorten the expression, we obtain

$$\begin{aligned} \boldsymbol{\mathcal{M}}^T\boldsymbol{\Lambda}_s &= \boldsymbol{\Lambda}_{n+1} + h_n\theta\boldsymbol{\lambda}_s^T\, \boldsymbol{f}_{\boldsymbol{uu}}(\boldsymbol{u}_{n+1})\boxed{\frac{d\boldsymbol{u}_{n+1}}{d\boldsymbol{\eta}}\boldsymbol{v}} + h_n\theta\boldsymbol{f}_{\boldsymbol{u}}^T(\boldsymbol{u}_{n+1})\boldsymbol{\Lambda}_s \\ \boldsymbol{\Lambda}_n &= \boldsymbol{\mathcal{M}}^T\boldsymbol{\Lambda}_s + h_n(1-\theta)\boldsymbol{\lambda}_s^T\boldsymbol{f}_{\boldsymbol{uu}}(\boldsymbol{u}_n)\boxed{\frac{d\boldsymbol{u}_n}{d\boldsymbol{\eta}}\boldsymbol{v}} + h_n(1-\theta)\boldsymbol{f}_{\boldsymbol{u}}^T(\boldsymbol{u}_n)\boldsymbol{\Lambda}_s, \end{aligned} \tag{2.23}$$

with the terminal condition

$$\boldsymbol{\Lambda}_N = \frac{d}{d\boldsymbol{u}}\left(\frac{d\psi}{d\boldsymbol{u}}(\boldsymbol{u}_n)\right)^T \frac{\partial \boldsymbol{u}_n}{\partial \boldsymbol{\eta}}\boldsymbol{v}. \tag{2.24}$$

Comparing the second-order adjoint (2.23) with the first-order adjoint (2.13), one can see that they are similar; the only difference is the additional term containing the Hessian-vector product of the DAE right-hand side. They result in linear systems with the same shifted Jacobian matrix $\boldsymbol{\mathcal{M}}^T - h_n\theta\boldsymbol{f}_{\boldsymbol{u}}^T(\boldsymbol{u}_{n+1})$ but different right-hand sides. Therefore, they can be solved together with those in the first-order adjoint, using the same preconditioners.

For large scale simulations, computing the full forward sensitivity matrix $\frac{d\boldsymbol{u}_n}{d\boldsymbol{\eta}}$ quickly becomes impractical because it requires a computational cost that is linear with the number of states. However, calculating the directional derivatives for the forward sensitivities (boxed terms in (2.23)) makes the cost constant; as a result, the computational cost of the second-order adjoint is independent of number of inputs (states and parameters), like the cost of the first-order adjoint.

2.3.4. Second-order adjoint: sensitivities to parameters. To obtain the parameter sensitivities and incorporate cases where there are integral terms in the objective function, we can apply techniques similar to these used above to extend the original DAE to a new system

$$\underline{\boldsymbol{\mathcal{M}}}\dot{\underline{\boldsymbol{u}}} = \underline{F}(t, \underline{\boldsymbol{u}}),\ t \in [t_0, t_F] \tag{2.25}$$

where

$$\underline{\boldsymbol{\mathcal{M}}} = \begin{bmatrix} \boldsymbol{\mathcal{M}} & & \\ & \boldsymbol{I}_{N_p\times N_p} & \\ & & 1 \end{bmatrix}, \underline{\boldsymbol{u}} = \begin{bmatrix} \boldsymbol{u} \\ \boldsymbol{p} \\ q \end{bmatrix}, \underline{F} = \begin{bmatrix} F \\ \boldsymbol{0}_{N_p\times 1} \\ r \end{bmatrix}.$$

The second equation enforces constant parameters during the time integration, and the last equation comes from a transformation of the integral (2.3).

In this extended framework, the initial condition is $\underline{\boldsymbol{\eta}}_0 = [\boldsymbol{\eta}\ \boldsymbol{p}\ 0]^T$. The extended Jacobian is

$$\underline{F}_{\underline{\boldsymbol{u}}} = \begin{bmatrix} \boldsymbol{f_u} & \boldsymbol{f_p} & \boldsymbol{0}_{N_d\times 1} \\ \boldsymbol{0}_{N_p\times N_d} & \boldsymbol{0}_{N_p\times N_p} & \boldsymbol{0}_{N_p\times 1} \\ r_{\boldsymbol{u}} & r_{\boldsymbol{p}} & 0 \end{bmatrix},$$

and the extended forward sensitivity matrix is given by

$$\frac{d\underline{\boldsymbol{u}}}{d\underline{\boldsymbol{\eta}}} = \begin{bmatrix} \frac{d\boldsymbol{u}}{d\boldsymbol{\eta}} & \frac{d\boldsymbol{u}}{d\boldsymbol{p}} & \boldsymbol{0}_{N_d\times 1} \\ \boldsymbol{0}_{N_p\times N_d} & \boldsymbol{I}_{N_p\times N_p} & \boldsymbol{0}_{N_p\times 1} \\ \frac{dq}{d\boldsymbol{\eta}} & \frac{dq}{d\boldsymbol{p}} & 0 \end{bmatrix}.$$

The first-order adjoint variable expands to the combination of three variables, corresponding to the partial derivative of the objective function with respect to the initial condition of the system state, the parameters, and the initial value of q, respectively. The third variable has a constant value 1 because of the zeros in the last column of $\underline{F}_{\underline{\boldsymbol{u}}}$ (see the Appendix in [36]).

The extended Hessian of the DAE right-hand side contains $3\times 3\times 3$ tensor blocks, including $\boldsymbol{f_{uu}}$, $F_{\boldsymbol{up}}$, $F_{\boldsymbol{pu}}$, $F_{\boldsymbol{pp}}$, $r_{\boldsymbol{uu}}$, $r_{\boldsymbol{up}}$, $r_{\boldsymbol{pu}}$, $r_{\boldsymbol{pp}}$, and 19 zero blocks. The vector-Hessian product term in (2.21), $\boldsymbol{\lambda}_s^T \boldsymbol{f_{uu}}(\boldsymbol{u}_n)$ is

$$\begin{bmatrix} \boldsymbol{\lambda}^T\boldsymbol{f_{uu}} + r_{\boldsymbol{uu}} & \boldsymbol{\lambda}^T\boldsymbol{f_{up}} + r_{\boldsymbol{up}} & \boldsymbol{0} \\ \boldsymbol{\lambda}^T\boldsymbol{f_{pu}} + r_{\boldsymbol{pu}} & \boldsymbol{\lambda}^T\boldsymbol{f_{pp}} + r_{\boldsymbol{pp}} & \boldsymbol{0} \\ 0 & 0 & 0 \end{bmatrix}.$$

We also need to extend the second-order adjoint variable multiplied with a directional vector to three variables denoted by $\boldsymbol{\Lambda}$, $\boldsymbol{\Gamma}$ and Θ. The corresponding directional vector should be split into three components $\boldsymbol{v}_1 \in \mathbb{R}^{N_d}$,$\boldsymbol{v}_2 \in \mathbb{R}^{N_p}$, and $\boldsymbol{v}_3 \in \mathbb{R}^1$. We define the new directional forward sensitivity to $\boldsymbol{w}_1 \in \mathbb{R}^{N_d}, \boldsymbol{w}_2 \in \mathbb{R}^{N_p}, \boldsymbol{w}_3 \in \mathbb{R}^1$ for the boxed term in (2.23) where

$$\begin{bmatrix} \boldsymbol{w}_1(\boldsymbol{u}_n) \\ \boldsymbol{w}_2(\boldsymbol{u}_n) \\ \boldsymbol{w}_3(\boldsymbol{u}_n) \end{bmatrix} = \frac{d\underline{\boldsymbol{u}}_n}{d\underline{\boldsymbol{\eta}}} \begin{bmatrix} \boldsymbol{v}_1 \\ \boldsymbol{v}_2 \\ \boldsymbol{v}_3 \end{bmatrix}.$$

Multiplying the vector-Hessian product term with the directional forward sensitivities eliminates $\boldsymbol{w}_3$ because of the zeros in the last row and leads to $\boldsymbol{w}_2 = \boldsymbol{v}_2$ because of the identity in the center. Thus only $\boldsymbol{w}_1$ needs to be obtained with TLMs. See the supplementary material for details.

$$\begin{aligned} \boldsymbol{\mathcal{M}} \boldsymbol{w}_{n+1} = \boldsymbol{\mathcal{M}} \boldsymbol{w}_n + h_n\big((1-\theta)\left(\boldsymbol{f_u}(\boldsymbol{u}_n)\boldsymbol{w}_n + \boldsymbol{f_p}(\boldsymbol{u}_n)\boldsymbol{v}_2\right) \\ + \theta\left(\boldsymbol{f_u}(\boldsymbol{u}_{n+1})\boldsymbol{w}_{n+1} + \boldsymbol{f_p}(\boldsymbol{u}_{n+1})\boldsymbol{v}_2\right)\big). \end{aligned} \tag{2.26}$$

Expanding the augmented system leads to

$$
\begin{aligned}
\boldsymbol{\mathcal{M}}^T\,\boldsymbol{\Lambda}_s &= \boldsymbol{\Lambda}_{n+1} + h_n\theta\, \boldsymbol{f}_{\boldsymbol{u}}^T(\boldsymbol{u}_{n+1})\,\boldsymbol{\Lambda}_s \\
&\quad + h_n\theta\left(\boldsymbol{\lambda}_s^T\,\boldsymbol{f}_{\boldsymbol{uu}}(\boldsymbol{u}_{n+1})\boldsymbol{w}_1(\boldsymbol{u}_{n+1}) + r_{\boldsymbol{uu}}(\boldsymbol{u}_{n+1})\boldsymbol{w}_1(\boldsymbol{u}_{n+1})\right) \\
&\quad + h_n\theta\left(\boldsymbol{\lambda}_s^T\,\boldsymbol{f}_{\boldsymbol{up}}(\boldsymbol{u}_{n+1})\boldsymbol{w}_2(\boldsymbol{u}_{n+1}) + r_{\boldsymbol{up}}(\boldsymbol{u}_{n+1})\boldsymbol{w}_2(\boldsymbol{u}_{n+1})\right) \\
\boldsymbol{\Lambda}_n &= \boldsymbol{\mathcal{M}}^T\,\boldsymbol{\Lambda}_s + h_n(1-\theta)\boldsymbol{f}_{\boldsymbol{u}}^T(\boldsymbol{u}_n)\boldsymbol{\Lambda}_s \\
&\quad + h_n(1-\theta)\left(\boldsymbol{\lambda}_s^T\,\boldsymbol{f}_{\boldsymbol{uu}}(\boldsymbol{u}_n)\boldsymbol{w}_1(\boldsymbol{u}_n) + r_{\boldsymbol{uu}}(\boldsymbol{u}_n)\boldsymbol{w}_1(\boldsymbol{u}_n)\right) \\
&\quad + h_n(1-\theta)\left(\boldsymbol{\lambda}_s^T\,\boldsymbol{f}_{\boldsymbol{up}}(\boldsymbol{u}_n)\boldsymbol{w}_2(\boldsymbol{u}_n) + r_{\boldsymbol{up}}(\boldsymbol{u}_n)\boldsymbol{w}_2(\boldsymbol{u}_n)\right) \\
\boldsymbol{\Gamma}_n &= \boldsymbol{\Gamma}_{n+1} + h_n\theta\boldsymbol{f}_{\boldsymbol{p}}^T(\boldsymbol{u}_{n+1})\,\boldsymbol{\Lambda}_s \\
&\quad + h_n\theta\left(\boldsymbol{\lambda}_s^T\,\boldsymbol{f}_{\boldsymbol{pu}}(\boldsymbol{u}_{n+1})\boldsymbol{w}_1(\boldsymbol{u}_{n+1}) + r_{\boldsymbol{pu}}(\boldsymbol{u}_{n+1})\boldsymbol{w}_1(\boldsymbol{u}_{n+1})\right) \\
&\quad + h_n\theta\left(\boldsymbol{\lambda}_s^T\,\boldsymbol{f}_{\boldsymbol{pp}}(\boldsymbol{u}_{n+1})\boldsymbol{w}_2(\boldsymbol{u}_{n+1}) + r_{\boldsymbol{pp}}(\boldsymbol{u}_{n+1})\boldsymbol{w}_2(\boldsymbol{u}_{n+1})\right) \\
&\quad + h_n(1-\theta)\boldsymbol{f}_{\boldsymbol{p}}^T(\boldsymbol{u}_n)\,\boldsymbol{\Lambda}_s \\
&\quad + h_n(1-\theta)\left(\boldsymbol{\lambda}_s^T\,\boldsymbol{f}_{\boldsymbol{pu}}(\boldsymbol{u}_n)\,\boldsymbol{w}_1(\boldsymbol{u}_n) + r_{\boldsymbol{pu}}(\boldsymbol{u}_n)\boldsymbol{w}_1(\boldsymbol{u}_n)\right) \\
&\quad + h_n(1-\theta)\left(\boldsymbol{\lambda}_s^T\,\boldsymbol{f}_{\boldsymbol{pp}}(\boldsymbol{u}_n)\,\boldsymbol{w}_2(\boldsymbol{u}_n) + r_{\boldsymbol{pp}}(\boldsymbol{u}_n)\boldsymbol{w}_2(\boldsymbol{u}_n)\right) \\
\Theta_n &= \Theta_{n+1},
\end{aligned}
\tag{2.27}
$$

with terminal conditions

$$
\begin{aligned}
\boldsymbol{\Lambda}_N &= \frac{\partial}{\partial \boldsymbol{u}}\left(\frac{\partial \psi}{\partial \boldsymbol{u}}(\boldsymbol{u}_n)\right)^T \frac{\partial \boldsymbol{u}_n}{\partial \boldsymbol{\eta}}\boldsymbol{v}_1 + \left(\frac{\partial}{\partial \boldsymbol{u}}\left(\frac{\partial \psi}{\partial \boldsymbol{u}}(\boldsymbol{u}_n)\right)^T \frac{\partial \boldsymbol{u}_n}{\partial \boldsymbol{p}} + \frac{\partial}{\partial p}\left(\frac{\partial \psi}{\partial \boldsymbol{u}}(\boldsymbol{u}_n)\right)^T\right)\boldsymbol{v}_2 \\
\boldsymbol{\Gamma}_N &= \frac{\partial}{\partial \boldsymbol{u}}\left(\frac{\partial \psi}{\partial p}(\boldsymbol{u}_n)\right)^T \frac{\partial \boldsymbol{u}_n}{\partial \boldsymbol{\eta}}\boldsymbol{v}_1 + \left(\frac{\partial}{\partial \boldsymbol{u}}\left(\frac{\partial \psi}{\partial p}(\boldsymbol{u}_n)\right)^T \frac{\partial \boldsymbol{u}_n}{\partial \boldsymbol{p}} + \frac{\partial}{\partial p}\left(\frac{\partial \psi}{\partial p}(\boldsymbol{u}_n)\right)^T\right)\boldsymbol{v}_2.
\end{aligned}
\tag{2.28}
$$

The final solution is given by

$$
\begin{aligned}
\boldsymbol{\Lambda}_0 &= \frac{\partial}{\partial \boldsymbol{\eta}}\left(\frac{\partial \psi}{\partial \boldsymbol{\eta}}\right)^T \boldsymbol{v}_1 + \frac{\partial}{\partial \boldsymbol{p}}\left(\frac{\partial \psi}{\partial \boldsymbol{\eta}}\right)^T \boldsymbol{v}_2 \\
\boldsymbol{\Gamma}_0 &= \frac{\partial}{\partial \boldsymbol{\eta}}\left(\frac{\partial \psi}{\partial \boldsymbol{p}}\right)^T \boldsymbol{v}_1 + \frac{\partial}{\partial \boldsymbol{p}}\left(\frac{\partial \psi}{\partial \boldsymbol{p}}\right)^T \boldsymbol{v}_2.
\end{aligned}
\tag{2.29}
$$

To compute the total derivatives for ψ, we can apply the chain rule with the adjoint solution

$$
\nabla_{\boldsymbol{p}}\psi = \left(\frac{d\psi}{d\boldsymbol{p}}\right)^T = \left(\frac{d\boldsymbol{\eta}}{d\boldsymbol{p}}\right)^T \left(\frac{\partial \psi}{\partial \boldsymbol{\eta}}\right)^T + \left(\frac{\partial \psi}{\partial \boldsymbol{p}}\right)^T = \boldsymbol{\eta}_p^T\boldsymbol{\lambda}_0 + \boldsymbol{\mu}_0. \tag{2.30}
$$

Similarly the second-order directional derivative with respect to the parameters can

be computed as
(2.31)

$$\begin{aligned}\nabla^2_{\boldsymbol{p}}\psi\,\boldsymbol{\sigma} &= \frac{d}{d\boldsymbol{p}}\left(\frac{d\psi}{d\boldsymbol{p}}\right)^T\boldsymbol{\sigma}\\ &= \frac{\partial\psi}{\partial\boldsymbol{\eta}}\boldsymbol{\eta}_{\boldsymbol{pp}}\,\boldsymbol{\sigma} + \boldsymbol{\eta}_{\boldsymbol{p}}^T\left(\frac{\partial}{\partial\boldsymbol{\eta}}\left(\frac{\partial\psi}{\partial\boldsymbol{\eta}}\right)^T\boldsymbol{\eta}_{\boldsymbol{p}} + \frac{\partial}{\partial\boldsymbol{p}}\left(\frac{\partial\psi}{\partial\boldsymbol{\eta}}\right)^T\right)\boldsymbol{\sigma} + \frac{\partial}{\partial\boldsymbol{\eta}}\left(\frac{\partial\psi}{\partial\boldsymbol{p}}\right)^T\boldsymbol{\eta}_{\boldsymbol{p}}\,\boldsymbol{\sigma}\\ &+ \frac{\partial}{\partial\boldsymbol{p}}\left(\frac{\partial\psi}{\partial\boldsymbol{p}}\right)^T\boldsymbol{\sigma}\\ &= \boldsymbol{\lambda}_0^T\,\boldsymbol{\eta}_{\boldsymbol{pp}}\,\boldsymbol{\sigma} + \boldsymbol{\eta}_{\boldsymbol{p}}^T\,\boldsymbol{\Lambda}_0 + \boldsymbol{\Gamma}_0\end{aligned}$$

with $\boldsymbol{v}_1 = \boldsymbol{\eta}_{\boldsymbol{p}}\boldsymbol{\sigma}$ and $\boldsymbol{v}_2 = \boldsymbol{\sigma}$. At this point the second-order derivative to initial values is simply

$$\nabla^2_{\boldsymbol{\eta}}\psi\,\boldsymbol{\sigma} = \frac{d}{d\boldsymbol{\eta}}\left(\frac{d\psi}{d\boldsymbol{\eta}}\right)^T\boldsymbol{\sigma} = \boldsymbol{\Lambda}_0, \tag{2.32}$$

with $\boldsymbol{v}_1 = \boldsymbol{\sigma}$.

3. PETSc TSAdjoint.

We begin this section with an overview of the software `PETSc TSAdjoint`, and then discuss the design and user interface as well as some implementation issues.

3.1. Overview of the software.

`PETSc` is a scalable MPI and GPU-based object-oriented numerical software library written in C and fully usable from C, C++, Fortran, and Python. It is publicly available at https://www.mcs.anl.gov/petsc/. `PETSc` has several fundamental classes from which applications are composed, including data structures for vectors and matrices, abstractions for working with subspaces of vectors, linear and nonlinear solvers, ODE/DAE solvers, and optimization solvers (within the Toolkit for Advanced Optimization (`TAO`) component of `PETSc`). In addition, `PETSc` has an abstract class DM that serves as an adapter between meshes, discretizations, and other problem descriptors and the algebraic and timestepping objects that are used to solve the discrete problem.

`PETSc TSAdjoint` provides a number of advantages. It avoids the full differentiation of a simulation code that classic AD requires, while maintaining the accuracy and speed of using AD tools. `PETSc` also offers finite-difference approximations for gradient computations, which can be used to generate Jacobian matrices (or Jacobian-vector products in a matrix-free context), as well as to validate the user-supplied Jacobian and even the adjoint sensitivities. Users can easily enable these functionalities via command line options at runtime. Compared with the continuous adjoint approach [19] that has been popular in control theory for a long time, the discrete adjoint approach adopted in `PETSc` does not require users to derive a new set of PDEs and determine boundary conditions to ensure the existence of the solution of the adjoint equations. One may argue that the continuous adjoint approach allows different discretization schemes to be applied to the adjoint equation, giving opportunities for efficiency improvement. However, adapting spatial discretization is not trivial, since it may involve changes to the mesh and need extra code development to implement the new schemes. And interpolation in both spatial and temporal domain becomes necessary because the checkpointed data from the original forward model cannot be used directly in solving the continuous adjoint equation. The interpolation will also induce numerical errors and uncertainty. Thus, exploiting the flexibility in choosing discretization schemes for continuous adjoint approaches can be a tremendous burden for application developers. The abstraction level at which the discrete adjoint model in `PETSc` is derived provides a balance between flexibility and usability—it does not raise concerns on discretization, and it still offers flexibility in selection of algebraic solvers.

Furthermore, various checkpointing schemes have been implemented in a new class called `TSTrajectory` which generates an optimal checkpointing schedule used internally by `TSAdjoint`, thus being completely transparent to users. Using an optimal checkpointing schedule is critical for achieving good performance in adjoint calculations. It is a difficult combinatorial problem and orthogonal to the focus of application developers. Therefore, the implementation of automatic checkpointing is a major advantage to application developers.

3.2. Design and user interface. Rooted in the `PETSc` timestepping library [1], `TSAdjoint` has C, Fortran, and Python interfaces and is designed primarily for the scalable computation of sensitivities of systems of time-dependent PDEs, DAEs, and ODEs. For each class of time integration methods in PETSc, a corresponding adjoint version of the algorithm is implemented with the context (e.g., method coefficients, working vectors) shared with the forward timestepping solver. The adjoint solvers are provided with event detection and handling (`TSEvents`), solution monitoring (`TSMonitor`), and performance profiling and thus are feature-complete compared with their counterparts. The event feature is particularly important for handling hybrid dynamical systems with discontinuities (or jumps) in time. These problems are known to be challenging for sensitivity analysis because complicated jump conditions at the switching surface need to be derived and implemented. Interested readers can refer to [34] for details on how this capability is achieved with `PETSc TSAdjoint`.

In `PETSc`, DAEs and ODEs are formulated as $\boldsymbol{F}(t, \boldsymbol{u}, \dot{\boldsymbol{u}}) = \boldsymbol{G}(t, \boldsymbol{u})$. For clarity of presentation, the form considered in this paper (2.1) is a common case where $\boldsymbol{F} = \boldsymbol{\mathcal{M}}\dot{\boldsymbol{u}} - \boldsymbol{f}$ and $\boldsymbol{G} = \boldsymbol{0}$, but `TSAdjoint` is extensible to fully support the more general case. To use the `PETSc` integrators, users supply callback routines for the residual function ($\boldsymbol{F}$ and $\boldsymbol{G}$) evaluations, and optional routines for Jacobian evaluation when implicit methods are chosen. For example, the Jacobian to the state for (2.1), by the chain rule, is $a\boldsymbol{F}_{\dot{\boldsymbol{u}}} + \boldsymbol{F}_{\boldsymbol{u}}$, where the shift parameter a depends on the time integration method and is passed to users. For sensitivity analysis, these same callbacks are reused, but a few additional callbacks may be required in order to provide derivatives (Jacobian and Hessian) of the ODE/DAE operator with respect to system state or parameters depending on the application needs. The Jacobian can be given either directly or in matrix-free form. The matrix-free form (vector-Hessian-vector product) is preferred for the Hessian because the sensitivity analysis techniques do not need to use the matrix or tensor directly, the memory footprint can be dramatically reduced, and the vector-Hessian-vector product can be generated much more efficiently by AD tools than can the Hessian itself. The vectors to be multiplied with the Hessian are also prepared by `PETSc` and accessed by users through the API. Table 1 summarizes the callback routines for several typical use cases.

The user interface to the adjoint solver is consistent with that of the timestepping solver. In particular, users need to create the appropriate `PETSc` vectors for storing the adjoint variables, provide the problem-specific context using `TSSetCostGradients()` for first-order adjoints, and initialize the adjoint variables according to the proper terminal conditions between the end of the forward solve and the start of the adjoint solve. For the second-order adjoint, additional adjoint variables need to be provided

Table 1: User-supplied callbacks for an implicit timestepping solver and its adjoint calculations. Reusable callbacks across use cases are marked in gray.

Use case	Without integral			With integral (2.3)		
forward integration	$\boldsymbol{\mathcal{M}}\dot{\boldsymbol{u}} - \boldsymbol{f}$ $a\boldsymbol{\mathcal{M}} - \boldsymbol{f}_{\boldsymbol{u}}$			r		
1st-order adjoint or TLM	$\mathcal{M}\dot{u} - f$ $a\mathcal{M} - f_u$	$-\boldsymbol{f}_{\boldsymbol{p}}$		r	$r_{\boldsymbol{u}}$ $r_{\boldsymbol{p}}$	
2nd-order adjoint	$\mathcal{M}\dot{u} - f$ $a\mathcal{M} - f_u$	$-f_p$	$-\boldsymbol{v}_1^T \boldsymbol{f}_{\boldsymbol{uu}} \boldsymbol{v}_2$ $-\boldsymbol{v}_1^T \boldsymbol{f}_{\boldsymbol{up}} \boldsymbol{v}_2$ $-\boldsymbol{v}_1^T \boldsymbol{f}_{\boldsymbol{pu}} \boldsymbol{v}_2$ $-\boldsymbol{v}_1^T \boldsymbol{f}_{\boldsymbol{pp}} \boldsymbol{v}_2$	r	r_u r_p	$r_{\boldsymbol{uu}} \boldsymbol{v}_3$ $r_{\boldsymbol{up}} \boldsymbol{v}_3$ $r_{\boldsymbol{pu}} \boldsymbol{v}_3$ $r_{\boldsymbol{pp}} \boldsymbol{v}_3$

using `TSSetCostHessianProducts()`, and tangent linear variables need to be set with `TSAdjointSetForward()`.

Adaptive timestepping is naturally supported. Both the tangent linear and adjoint solvers follow the same trajectory that is determined by the timestepping solver via a timestep controller. The `PETSc` timestepping solver provides a variety of options for automatic timestep control in order to attain a user-specified goal. The adaptivity logic can be based on embedded error estimates [11], linear digital control theory [28], the Courant-Friedrichs-Lewy (CFL) condition, and global error estimates [8]. When using adaptive timestepping, an online checkpointing scheme must be employed because the total number of steps is not known a priori.

3.3. Jacobian/Hessian computation.

`PETSc` provides several choices for the Jacobian/Hessian operators or their application needed for the forward and adjoint solvers. First, `PETSc` offers efficient and automatic Jacobian approximation with finite differences and coloring [13], if the Jacobian is not supplied by users, and the sparsity pattern of the Jacobian is available (e.g., when the `PETSc` data management object `DM` is used for the implementation of discretization schemes). Second, `PETSc` allows low-level AD tools to differentiate local routines so that MPI routines need not be differentiated through, and it provides utilities to facilitate fast Jacobian recovery from AD-generated matrices (see [31] for details). Third, one can use libraries such as Firedrake and FEniCS that have excellent high-level AD capabilities; this is demonstrated with examples in Section 5.

4. Checkpointing.

To calculate the discrete adjoint state, Jacobians and Hessians or matrix-free operations for them need to be evaluated by using the system states that are computed in the forward run. However, if all these values are retained, the storage space needed is proportional to the number of time steps performed. To overcome this drastic storage requirement, one must checkpoint selective states along the trajectory while recomputing the missing ones. This technique has been well studied in the literature. A notable offline algorithm, `revolve`, developed by Griewank and Walther [15], can generate a checkpointing schedule that minimizes the number of recomputation time steps, given the total number of time steps and the number of allowed checkpoints in memory. A C++ tool was developed to implement the `revolve` algorithm; and a few online algorithms [16, 30, 33] were also implemented for cases when the number of time steps is not known a priori; and a multistage algorithm were included to consider both disk and memory for storage [29]. Fig. 2a demonstrates an optimal schedule for adjoining 10 time steps given three checkpoints.

However, using these algorithms and the tool can cause difficulties. First, they provide only the schedule that guides the checkpoint manipulation for adjoint computation. Significant effort is still needed to implement the required operations that are dependent on the application codes and hardware platforms. For example, relevant questions include how to move the data to the designated storage media and in which format and how to change the workflow so that time steps could be recomputed between checkpoint access and adjoint state calculation. Second, the tool was designed to be an explicit controller for conducting forward integration and adjoint integration in time-dependent applications. Incorporating `revolve` in other simulation software such as `PETSc` can be intrusive, or even infeasible, especially when the integration package has its own adaptive timestep control and an established framework for time integration. Third, checkpointing only solution states at distinct time steps requires at least one recomputation before each adjoint step can be performed. This strategy is not necessarily ideal for the discrete adjoint of multistage time integration methods because checkpointing the intermediate stage values together with the solution states would remove the need to recompute the corresponding time steps.

To address these challenges, we have implemented the `TSTrajectory` component in `PETSc` to serve as the intermediary between `revolve` and the timestepping solver. It is responsible for implementing the operations required by `revolve` and handling the adjoint workflow. The main features are summarized below:

- Storing and restoring a checkpoint are implemented for different storage media. In memory, these operations are straightforward; on disk or other devices, data format and parallel I/O must be considered.
- Data points can be requested from `TSTrajectory` by specifying either the timestep number (a unique index for labeling each time step) or the time. The data point is restored directly if it has been checkpointed, or it is recomputed if it is not available immediately. This process is hidden from the requesting code (i.e., the adjoint solver).
- `TSTrajectory` interprets the schedule generated and reorganizes the sequence of operations. In particular, in the forward run and the recomputation stage it decides when to save a checkpoint, and in the backward run it determines how to prepare the requested data.
- For multistage time integration methods, `TSTrajectory` allows users to checkpoint stage values while it still guarantees minimal recomputation using a modified `revolve` schedule. See Fig. 2b for an illustration.

Although the workflow is not controlled directly by `revolve`, it is equivalent to the one scheduled by `revolve`, and it allows the timestepping loops in `TS` and `TSAdjoint` to be unchanged.

5. Examples.

In this section, we present four representative examples from a diverse of problems including ODEs, PDEs, and DAEs. The goals are to (1) illustrate the use of the `PETSc` `TSAdjoint` in outer-loop applications such as optimal control and inverse problems (2) demonstrate the efficiency and scalability of the implementation and (3) show the usability of `PETSc` `TSAdjoint` in other scientific computing libraries. To date, `TSAdjoint` has been applied in domains including power systems [34], data assimilation [7], and computational fluid dynamics [22]. These applications are not covered in this paper. We refer readers to these references for more information.

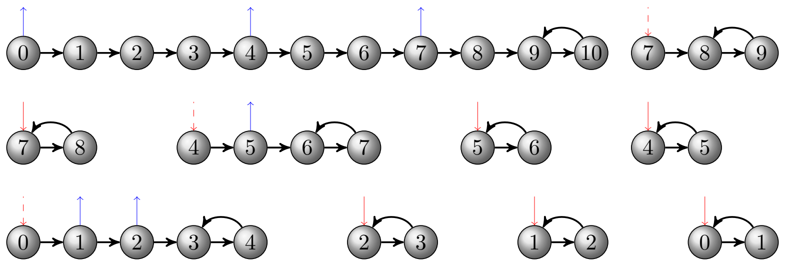

(a) Checkpoint only solutions.

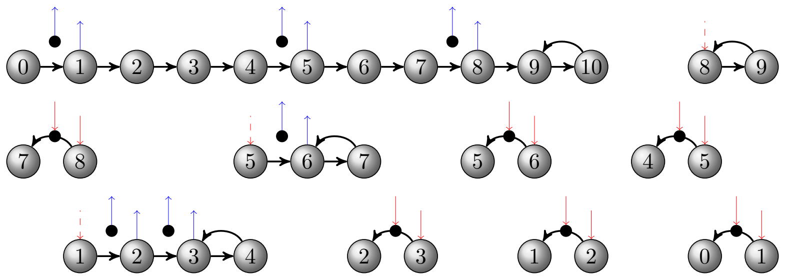

(b) Checkpoint both solutions and stage values (denoted by dots).

Fig. 2: From left to right, top to bottom: the processes controlled by (a) `revolve` and (b) modified `revolve`. The up arrow and down arrow stand for "store" operation and "restore" operation, respectively. When a stack is used for holding the checkpoints, the arrows with solid lines correspond to push and pop operations. The down arrow with dashed line indicates to read the top element on the stack without removing it.

5.1. An optimal control problem. aircraft trajectory planning is to find a control sequence that can control the pursuer to the targeting leader by minimizing a given cost function, as illustrated in Fig. 3a. The sequence is divided into finite time intervals $T_k = [t_k, t_{k+1}]$ for $k = 0, 1, \dots, N-1$. On each interval, control inputs are provided in response to the changes in the leader's position. The dynamics of the aircrafts is governed by a kinematic nonlinear model

$$\begin{aligned} \dot{x}_k(t) &= v_k(t)\cos(\omega_k(t)) \\ \dot{y}_k(t) &= v_k(t)\sin(\omega_k(t)) \end{aligned} \tag{5.1}$$

defined on each time interval T_k.

The problem can be transformed into the minimization of the cost function

$$\psi(\boldsymbol{u}, \boldsymbol{p}) = \int_0^{t_F} \|\boldsymbol{u}(t) - \boldsymbol{u}_{\texttt{leader}}(t)\| dt,\ \ \boldsymbol{u} = [x(t), y(t)]^T,\ \ \boldsymbol{p} = [v(t), \omega(t)]^T \tag{5.2}$$

subject to dynamical constraints (5.1) and inequality constraints

$$v_{\texttt{min}} \le v(t) \le v_{\texttt{max}}, \quad \omega_{\texttt{min}} \le \omega(t) \le \omega_{\texttt{max}}. \tag{5.3}$$

This is a simple example from [25] but has all the complexities including nonlinearity and inequality constraints that are common for practical dynamical optimal

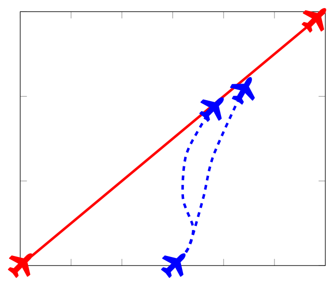

(a) Trajectories of the leader and the pursuer.

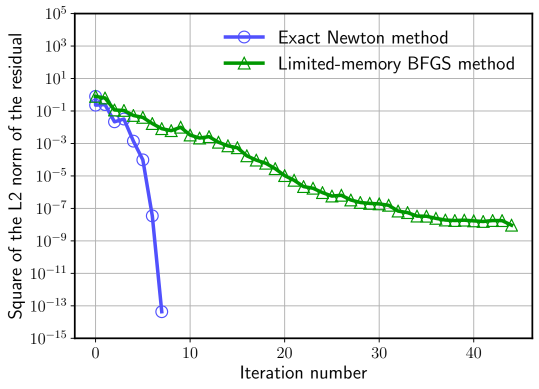

(b) Convergence of the optimization methods.

Fig. 3: Aircraft trajectory planning: (a) possible solutions to the problem, and (b) comparision in convergence between the limited-memory BFGS method and the Newton method with the exact Hessian in matrix-free form.

control applications. We implemented this example in PETSc using PETSc time integrators for solving the dynamical system and using TAO for the optimization. For optimization, the first-order derivative information (that is, the gradient) required by gradient-based Newton methods is obtained with the first-order adjoint solver, while the second-order derivative information (contained in the Hessian-vector product) is obtained with the second-order adjoint solver and used with matrix-free exact Newton methods.

Fig. 3b shows that the second-order derivative calculated with the PETSc adjoint solver speeds up the convergence of the optimization significantly: the exact Newton method takes 7 iterations to drive the norm of the gradient of the objective function below 10^{-13}, whereas the classic limited-memory Broyden-Fletcher-Goldfarb-Shanno (BFGS) method [5] approached 10^{-8} after 50 iterations.

5.2. An inverse initial value problem. This example demonstrates the application of adjoint methods in an inverse problem of recovering the initial condition for a time-dependent PDE, and the parallel performance of the adjoint calculation involved. The problem can be formulated as a PDE-constrained optimization problem that minimizes the discrepancy between the simulated result and observation data (reference solution):

$$\underset{\boldsymbol{U}_0}{\text{minimize}} \, \|\boldsymbol{U}(t_f) - \boldsymbol{U}^{ob}(t_f)\|_2 \tag{5.4}$$

subject to the Gray-Scott equations [18]

$$\begin{aligned} \dot{\mathbf{u}} &= D_1 \nabla^2 \mathbf{u} - \mathbf{u}\mathbf{v}^2 + \Delta\gamma(1-\mathbf{u}) \\ \dot{\mathbf{v}} &= D_2 \nabla^2 \mathbf{v} + \mathbf{u}\mathbf{v}^2 - \Delta(\gamma+\kappa)\mathbf{v}, \end{aligned} \tag{5.5}$$

where $\boldsymbol{U} = [\mathbf{u}; \mathbf{v}]$ is the PDE solution vector and $\boldsymbol{U}_0$ is the initial condition. The PDE models the reaction and diffusion of two interacting species that produce spatial patterns over time, as shown in Fig. 4.

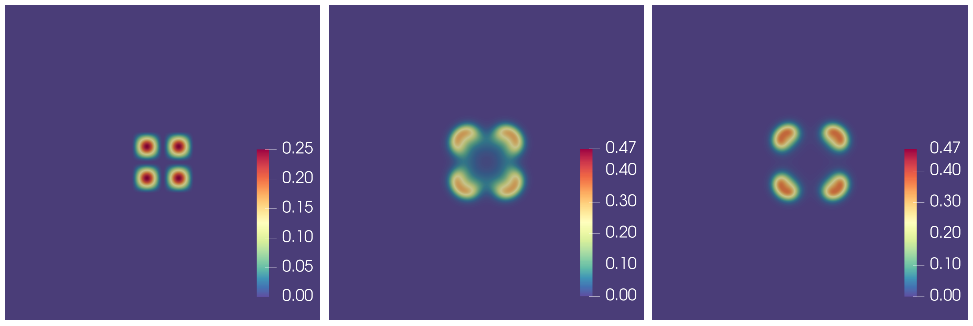

(a) t=0 sec (b) t=100 sec (c) t=200 sec

Fig. 4: Evoling spatial patterns of the concentrations v in the Gray-Scott equations.

Table 2: Performance comparison for two different Jacobian evaluation strategies and three selective timestepping methods. The grid size used in the tests is 100×100. A fix stepsize of 0.5 is used on the time interval $[0, 5]$.

Jacobian	Time integration	Wall time (s)	Ratio (adjoint/forward)	Iterations	First-order computations	RHS evaluations	Jacobian evaluations
Analytical	Backward Euler	30.0	0.48	188	194	5,870	5,870
	Crank-Nicolson	45.4	0.76	253	264	10,581	10,581
	Runge-Kutta 4	25.6	38.03	246	253	10,120	10,120
FDColoring	Backward Euler	19.9	0.48	188	196	67,190	-
	Crank-Nicolson	28.8	0.66	246	254	127,252	-
	Runge-Kutta 4	11.8	16.48	244	255	122,400	-

In our simulation, the PDE is solved with the method of lines approach. A centered finite-difference scheme is used for spatial discretization. The computational domain is $\Omega \in [0, 2]^2$. The time interval is $[t_0, t_f] = [0, 5]$. The reference solution is generated from the initial condition

$$\mathbf{u}_0 = 1 - 2\mathbf{v}_0, \quad \mathbf{v}_0 = \begin{cases} \sin^2(4\pi x)\cos^2(4\pi y)/4, \ \forall x, y \in [1.0, 1.5] \\ 0, \ \text{otherwise.} \end{cases} \tag{5.6}$$

To solve the optimization problem, we use the limited-memory BFGS algorithm [5] in `TAO` [10] by providing to `TAO` a function that returns the value of the objective function and its gradient with respect to U_0. The function is computed with a forward solve solving the PDE for solution and evaluation of the objective function, followed by an adjoint solve calculating the gradient expressed by (2.30).

Efficiency The efficiency of the adjoint solver can be defined by the ratio of the cost of the forward solve to the cost of the adjoint solve. The results for three timestepping methods are presented in Table 2.

The two selected implicit methods, backward Euler and Crank-Nicolson, are special cases of the theta method ($\theta = 1/2$ for backward Euler and $\theta = 0$ for Crank-Nicolson). Both achieve an efficiency ratio of less than 1. For linear problems, the optimal ratio is 1, assuming the cost of assembling the linear system and the right-hand side is identical and the cost of solving the transposed linear system in an adjoint time step is equivalent to the cost of solving the system in the corresponding forward time step. For nonlinear problems, a smaller ratio is expected because the forward solve requires the solution of one or more (depending on the timestepping algorithm) nonlinear systems while the adjoint run requires only the solution of linear systems at each adjoint time step, the number of which is the same as the number of nonlinear systems required in the forward time step. In this example, the nonlinear solve takes 2 Newton iterations on average. The adjoint solver based on backward Euler is slightly more efficient than the adjoint solver based on Crank-Nicolson because the Jacobian evaluation needed in equation (2.13b) can be avoided for backward Euler when the mass matrix is the identity. This kind of performance optimization can be discovered easily from the formula and implemented; however, it is difficult to be realized by algorithmic differentiation tools.

The fourth-order explicit method, Runge-Kutta 4, has a relatively high efficiency ratio, mainly because the right-hand side evaluation is significantly faster than the Jacobian evaluation, which consists of costly memory operations including assembling the matrix. Note that the Jacobian does not have to be provided in explicit form, `PETSc` supports the matrix-free Jacobian for which users only need to implement the application of the Jacobian to a given vector. Despite the high efficiency ratio, the explicit method is still the most efficient option for this problem since the (transposed) matrix-vector multiplication needed in the adjoint is considerably cheaper than solving an implicit system.

Interestingly, using finite differences and coloring outperforms the analytical Jacobian for this example and implementation. As Table 2 indicates, the number of iterations of the optimization process does not vary much between the two choices. The Jacobian approximation takes 10 right-hand side function evaluations (5 colors and 2 components in the PDE). Although more arithmetic operations are needed by finite differences, the array of values generated from the approximation can be transferred into a `PETSc` sparse matrix efficiently. In contrast, in the implementation of the analytical Jacobian the matrix values are set row-wise, which is natural for sparse matrices in the compressed sparse row format but less cache-efficient.

Parallel scaling. To demonstrate scalability of the adjoint solver, we ran the gradient calculation part of this benchmark problem with fine grid resolution on Argonne's supercomputer Theta, which is based on second-generation Intel Xeon Phi Knights Landing (KNL) processors. Each KNL node is assigned 64 MPI processes since there are 64 cores per node. Manually optimized linear algebra kernels (e.g., vectorized matrix-vector multiplication [35]) are used for best performance. Fig. 5 shows the scaling results for up to 8,192 MPI processes. Backward Euler and Crank-Nicolson achieve superlinear scalability in both the forward solve and the adjoint solve. The reason is that the convergence of the block Jacobi preconditioner depends on the number of processes and thus is not completely scalable. For Runge-Kutta 4 the scaling of the forward solve is not ideal because of the increasing communication cost in the right-hand side function evaluation as the number of processes increases. For the adjoint solve, however, perfect linear scalability is observed.

5.3. A libMesh example: adjoint of the Navier-Stokes equation. The example simulates low-speed incompressible fluid flow in a channel. The physics is governed by the Navier-Stokes equations on a domain $\Omega \in \mathcal{R}^2$, consisting of momentum and continuity equations

$$\begin{aligned} \dot{\boldsymbol{U}} + (\boldsymbol{U} \cdot \nabla)\boldsymbol{U} - \nu \Delta \boldsymbol{U} + \nabla \boldsymbol{P} &= 0 \\ \nabla \cdot \boldsymbol{U} &= 0, \end{aligned} \tag{5.7}$$

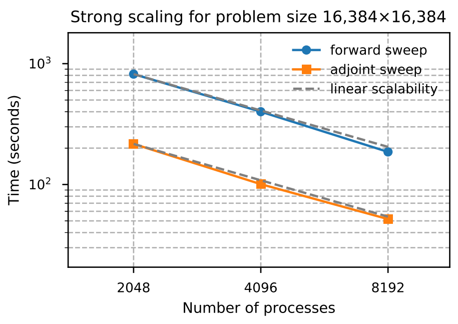

(a) Backward Euler

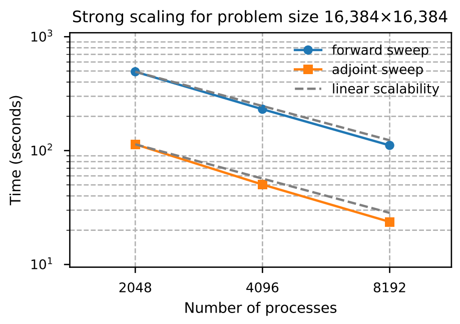

(b) Crank-Nicolson

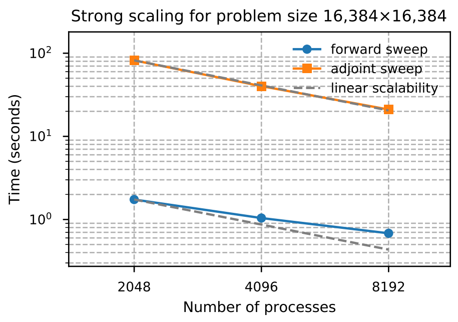

(c) Runge-Kutta 4

Fig. 5: Strong scaling of the adjoint sensitivity calculation for the 2D reaction-diffusion equation (5.5) on Argonne's supercomputer Theta. In all the tests, 32, 64 and 128 compute nodes with 64 MPI processes on each node are used. The grid size is $16,384 \times 16,384$ (yielding about 0.5 billion degrees of freedom). Three time integrations methods are tested. The linear systems are solved by using GMRES [27] with the block Jacobi preconditioner (and ILU(0) for each block).

where $\boldsymbol{U}$ is the velocity field, $\boldsymbol{P}$ is the pressure field, and ν is the kinematic viscosity. The geometry is a 100×20 rectangle discretized uniformly with $8,000$ quadrilateral elements composed of 4 nodes. The viscosity satisfies $\nu = 1$. For the velocity fields, periodic boundary condition are imposed at the right and left boundaries, and no-slip boundary conditions are imposed on the channel walls. The pressure is set to be a time-dependent function

$$\boldsymbol{P} = 0.01 * \sin(2\pi * t/50)$$

at the right boundary and a zero constant at the left boundary. This example is implemented in libMesh [20] Version 2.1 using second-order Lagrange elements. We have also implemented an interface to the `PETSc` TS component in order to use the adjoint solvers. After semi-discretization in space, the PDE is transformed into a system of DAEs, which is solved with the implicit timestepping solvers in PETSc. Since the DAEs are highly stiff, the linear system is solved with the sparse direct solver MUMPS [4] through PETSc.

For simplicity, we choose the functional to be the horizontal velocity at the central

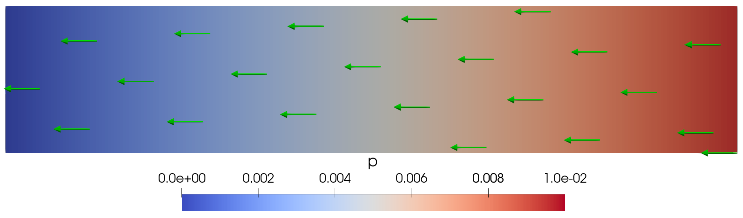

(a) Forward solution

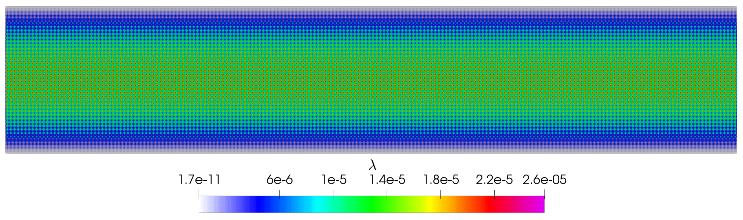

(b) Adjoint solution

Fig. 6: Navier-Stokes example: (a) pressure field in the solution at time $t = 60s$, where arrows denote the velocity vector, and (b) adjoint derivative of a functional (the horizontal velocity at the central node at the final time) with respect to the initial condition of the horizontal velocity field.

Table 3: Timings of the Navier-Stokes adjoint solver using libMesh.

Time integration	Stages	Wall time (s)	Ratio
Backward Euler	Forward model	18.4	1
	Adjoint model	14.6	0.78
Crank-Nicolson	Forward model	20.0	1
	Adjoint model	16.8	0.84

node at the final time and calculate its adjoint sensitivity with respect to the initial condition of the horizontal velocity field. Although this functional may not be physically interesting, it suffices to reflect the computational cost of the adjoint models for complicated functionals since the linear solves dominate the computational cost. For our configuration, the problem is in the almost linear regime; thus it takes one Newton iteration to converge for most forward time steps. The performance is shown in Table 3. The adjoint solve takes 78% of the cost of the forward solve for backward Euler and 84% for Crank-Nicolson, while a rough estimate of the theoretical performance ratio is 1 for both methods.

5.4. A Firedrake example: adjoint of the Burgers' equation. We consider the Burgers' equation on a uniform square mesh:

$$\begin{aligned} \dot{\boldsymbol{U}} + (\boldsymbol{U} \cdot \nabla)\boldsymbol{U} - \nu \Delta \boldsymbol{U} = 0 \\ (n \cdot \nabla)\boldsymbol{U} = 0 \text{ on } \Omega \end{aligned} \tag{5.8}$$

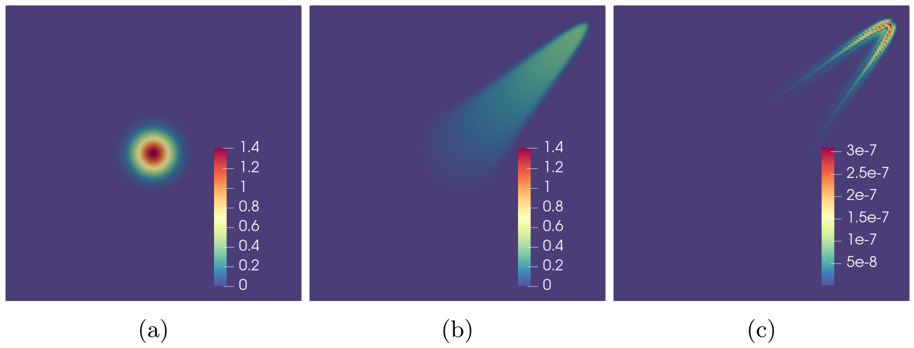

Fig. 7: Initial condition (a), final solution at $T = 2s$ (b), and sensitivity of $L2$ norm of error with respect to the intial condition (c).

Table 4: Timings of the Burgers' adjoint in Firedrake.

Time integration	Stages	Wall time (s)	Ratio	RHS evaluations	Jacobian evaluations
Backward Euler	Forward model	22.386	1	142	109
	Adjoint model	5.543	0.25	0	32
Crank-Nicolson	Forward model	40.704	1	254	157
	Adjoint model	5.868	0.14	0	32

where Ω is the domain boundary and ν is a constant scalar viscosity. The equation is discretized in space by using Lagrange finite elements of polynomial degree 2. The initial condition is a Gaussian profile with amplitude 1.0 and distribution width 0.06, as shown in Fig. 7, and 16 uniform time steps are used on the time interval $[0, 2]$ seconds. For testing, we compute the sensitivity of the error norm of the solution at the final time with respect to the initial condition, which is typically needed in data assimilation. A reference solution is computed by using a strict stepsize with the same settings. This example is implemented by using only a few lines of Python code. The right-hand side function and Jacobian function defining the ODE problem are automatically generated by specifying the variational formulations of the semi-discretized PDE using Firedrake; they are provided to the `PETSc` timestepping solver through `petsc4py` [9] for the forward and the adjoint solution.

Table 4 lists the total runtime and number of right-hand side and Jacobian evaluations for both the forward and the adjoint computation. We observe that the adjoint-to-forward ratios are 0.25 for backward Euler and 0.14 for Crank-Nicolson. While the runtime of the forward solve differs significantly for the time integration methods, the runtime of the adjoint solve is approximately the same. The reason is that the right-hand side function evaluation (the spatial discretization) dominates the total computational cost, while the adjoint solver of backward Euler or Crank-Nicolson takes the same number of Jacobian evaluations and the same number of linear solves (one per adjoint time step).

6. Conclusion. Algorithmic differentiation has long been needed by many scientific applications, especially as machine learning becomes increasingly popular. It has been realized at different levels of abstraction, posing different challenges for application developers and software developers. The new tool presented in this paper, `PETSc TSAdjoint`, provides an efficient and accurate approach for computing first-order and second-order adjoints for ODEs, DAEs, and time-dependent nonlinear PDEs. It makes the task of gradient calculation easier by avoiding full differentiation of the entire code, with no loss of accuracy and speed. Minimal changes are required for applications using `PETSc` time integrators to be equipped with sensitivity analysis capabilities. An optimal checkpointing component has been developed to deliver transparent and optimal checkpointing strategies on high-performance computing platforms. Parallelism is inherited from `PETSc` parallel infrastructures. Thanks to the hierarchical structure of `PETSc`, the adjoint solvers take advantage of the well-developed nonlinear and linear iterative solvers and the large collection of preconditioners in `PETSc`.

Extensive experiments have been performed to demonstrate the usability, efficiency and scalability of the adjoint solvers. We have shown that they can be easily used with a variety of other scientific computing libraries or tools in different programming languages. We have also shown that using finite differences and coloring and relying on high-level AD are efficient and convenient alternatives to deriving and implementing an analytical Jacobian. For first-order adjoints, the cost of the adjoint solve is typically less than the forward solve when implicit timestepping methods are employed. The performance ratio for explicit methods can exceed 1 if the Jacobian matrix is provided in the explicit form; however, this could be mitigated by using matrix-free implementations. Furthermore, the adjoint computation of PDEs scales nicely to large numbers of cores on a supercomputer, even when the scaling of the forward solve is not ideal. In addition, we show how the second-order adjoint sensitivities can be used to accelerate the convergence of optimization in an optimal control problem. Without doubt that Hessian-related information needed by second-order adjoints may be difficult to compute. However, `PETSc TSAdjoint` requires only a rank-1 vector-Hessian-vector product for the second-order adjoints.

As far as we know, this library is the first general-purpose HPC-friendly library that offers first-order and second-order discrete adjoint capabilities based on multistage time integration methods, supports sensitivity analysis for hybrid dynamical systems, and comes with sophisticated checkpointing support that is transparent to users. We expect that more applications in PDE-constrained optimization, data assimilation, uncertainty quantification, and machine learning will be enabled by our development.

Acknowledgments. We are grateful to Jed Brown for extensive code review and helpful disscusions during the development of the software. We would also like to thank Todd Munson for his valuable comments on the draft.

REFERENCES

[1] S. Abhyankar, J. Brown, E. M. Constantinescu, D. Ghosh, B. F. Smith, and H. Zhang, *PETSc/TS: a modern scalable ODE/DAE solver library*, arXiv e-preprints, (2018), https://arxiv.org/abs/1806.01437.

[2] M. Alexe and A. Sandu, *On the discrete adjoints of adaptive time stepping algorithms*, Journal of Computational and Applied Mathematics, 233 (2009), pp. 1005–1020, https://doi.org/https://doi.org/10.1016/j.cam.2009.08.109.

[3] M. S. Alnaes, J. Blechta, A. J. J. Hake, B. Kehlet, A. Logg, C. Richardson, J. Ring, M. E. Rognes, and G. N. Wells, *The FEniCS Project Version 1.5*, Archive of Numerical Software, (2015), https://doi.org/10.11588/ans.2015.100.20553.

[4] P. R. Amestoy, I. S. Duff, J. Koster, and J.-Y. L'Excellent, *A fully asynchronous multifrontal solver using distributed dynamic scheduling*, SIAM Journal on Matrix Analysis and

Applications, 23 (2001), pp. 15–41, https://doi.org/10.1137/S0895479899358194.

[5] S. J. Benson and J. J. More, *A limited memory variable metric method in subspaces and bound constrained optimization problems*, tech. report, in Subspaces and Bound Constrained Optimization Problems, 2001.

[6] C. H. Bischof, L. Roh, and A. J. Mauer-Oats, *ADIC: An extensible automatic differentiation tool for ANSI-C*, Software - Practice and Experience, 27 (1997), pp. 1427–1454, https://doi.org/10.1002/(SICI)1097-024X(199712)27:12⟨1427::AID-SPE138⟩3.0.CO;2-Q.

[7] L. Carracciuolo, E. M. Constantinescu, and L. D'Amore, *Validation of a PETSc based software implementing a 4DVAR data assimilation algorithm: a case study related with an oceanic model based on shallow water equation*, arXiv e-prints, (2018), https://arxiv.org/abs/1810.01361.

[8] E. M. Constantinescu, *Generalizing global error estimation for ordinary differential equations by using coupled time-stepping methods*, Journal of Computational and Applied Mathematics, 332 (2018), pp. 140–158, https://doi.org/https://doi.org/10.1016/j.cam.2017.05.012.

[9] L. D. Dalcin, R. R. Paz, P. A. Kler, and A. Cosimo, *Parallel distributed computing using Python*, Advances in Water Resources, 34 (2011), pp. 1124–1139, https://doi.org/10.1016/j.advwatres.2011.04.013.

[10] A. Dener and T. Munson, *Accelerating limited-memory quasi-newton convergence for large-scale optimization*, in Computational Science – ICCS 2019, vol. 11538 of Lecture Notes in Computer Science, Cham, 2019, Springer International Publishing, pp. 495–507.

[11] J. Dormand and P. Prince, *A family of embedded Runge-Kutta formulae*, Journal of Computational and Applied Mathematics, 6 (1980), pp. 19–26, https://doi.org/https://doi.org/10.1016/0771-050X(80)90013-3.

[12] P. E. Farrell, D. A. Ham, S. F. Funke, and M. E. Rognes, *Automated derivation of the adjoint of high-level transient finite element programs*, SIAM Journal on Scientific Computing, 35 (2013), pp. 369–393, https://doi.org/10.1137/120873558.

[13] A. H. Gebremedhin, F. Manne, and A. Pothen, *What color is your Jacobian? Graph coloring for computing derivatives*, SIAM Review, 47 (2005), pp. 629–705, https://doi.org/10.1137/S0036144504444711.

[14] R. Giering and T. Kaminski, *Recipes for adjoint code construction*, ACM Transactions on Mathematical Software, 24 (1998), pp. 437–474, https://doi.org/10.1145/293686.293695.

[15] A. Griewank and A. Walther, *Algorithm 799: revolve: an implementation of checkpointing for the reverse or adjoint mode of computational differentiation*, ACM Transactions on Mathematical Software, 26 (2000), pp. 19–45, https://doi.org/10.1145/347837.347846.

[16] V. Heuveline and A. Walther, *Online checkpointing for parallel adjoint computation in PDEs: application to goal-oriented adaptivity and flow control*, in Euro-Par 2006, vol. 4128 of Lecture Notes in Computer Science, Springer Berlin Heidelberg, 2006.

[17] A. C. Hindmarsh, P. N. Brown, K. E. Grant, S. L. Lee, R. Serban, D. E. Shumaker, and C. S. Woodward, *SUNDIALS: Suite of nonlinear and differential/algebraic equation solvers*, ACM Transactions on Mathematical Software, 31 (2005), pp. 363–396, https://doi.org/10.1145/1089014.1089020.

[18] W. Hundsdorfer and J. Verwer, *Numerical Solution of Time-Dependent Advection-Diffusion-Reaction Equations*, Springer Series in Computational Mathematics, Springer Berlin Heidelberg, 2007.

[19] A. Jameson, *Aerodynamic design via control theory*, Journal of Scientific Computing, 3 (1988), https://doi.org/10.1007/BF01061285.

[20] B. S. Kirk, J. W. Peterson, R. H. Stogner, and G. F. Carey, *libMesh: A C++ library for parallel adaptive mesh refinement/coarsening simulations*, Engineering with Computers, 22 (2006), pp. 237–254, https://doi.org/10.1007/s00366-006-0049-3.

[21] M. Lubin and I. Dunning, *Computing in operations research Using Julia*, INFORMS Journal on Computing, 27 (2015), pp. 238–248, https://doi.org/10.1287/ijoc.2014.0623.

[22] O. Marin, E. Constantinescu, and B. Smith, *Unsteady PDE-constrained optimization with spectral elements using PETSc and TAO*, arXiv e-prints, (2018), https://arxiv.org/abs/1806.01422.

[23] A. Paszke, S. Chintala, G. Chanan, Z. Lin, S. Gross, E. Yang, L. Antiga, Z. Devito, A. Lerer, and A. Desmaison, *Automatic differentiation in PyTorch*, 31st Conference on Neural Information Processing Systems, (2017), https://doi.org/10.1017/CBO9781107707221.009, https://arxiv.org/abs/arXiv:1011.1669v3.

[24] E. T. Phipps, R. A. Bartlett, D. M. Gay, and R. J. Hoekstra, *Large-scale transient sensitivity analysis of a radiation-damaged bipolar junction transistor via automatic differentiation*, in Advances in Automatic Differentiation, Springer Berlin Heidelberg, 2008, pp. 351–362.

[25] R. Raffard and C. Tomlin, *Second order adjoint-based optimization of ordinary and partial differential equations with application to air traffic flow*, Proceedings of the 2005, American Control Conference, (2005), pp. 798–803, https://doi.org/10.1109/ACC.2005.1470057.

[26] F. Rathgeber, D. A. Ham, L. Mitchell, M. Lange, F. Luporini, A. T. T. Mcrae, G.-T. Bercea, G. R. Markall, and P. H. J. Kelly, *Firedrake: Automating the finite element method by composing abstractions*, ACM Transactions on Mathematical Software, 43 (2016), pp. 24:1–24:27, https://doi.org/10.1145/2998441, http://doi.acm.org/10.1145/2998441.

[27] Y. Saad and M. H. Schultz, *GMRES: a generalized minimal residual algorithm for solving nonsymmetric linear systems*, SIAM Journal on Scientific and Statistical Computing, 7 (1986), pp. 856–869, https://doi.org/10.1137/0907058.

[28] G. Söderlind, *Digital filters in adaptive time-stepping*, ACM Transactions on Mathematical Software, 29 (2003), pp. 1–26, https://doi.org/10.1145/641876.641877.

[29] P. Stumm and A. Walther, *MultiStage approaches for optimal offline checkpointing*, SIAM Journal on Scientific Computing, 31 (2009), pp. 1946–1967, https://doi.org/10.1137/080718036.

[30] P. Stumm and A. Walther, *New algorithms for optimal online checkpointing*, SIAM Journal on Scientific Computing, 32 (2010), pp. 836–854.

[31] J. G. Wallwork, P. Hovland, H. Zhang, and O. Marin, *Computing derivatives for PETSc adjoint solvers using algorithmic differentiation*, arXiv e-prints, (2019), https://arxiv.org/abs/1909.02836.

[32] A. Walther and A. Griewank, *Getting started with ADOL-C*, in Combinatorial Scientific Computing, Chapman-Hall CRC Computational Science, 2012, pp. 181–202, https://doi.org/10.1201/b11644-8.

[33] Q. Wang, P. Moin, and G. Iaccarino, *Minimal repetition dynamic checkpointing algorithm for unsteady adjoint calculation*, SIAM Journal on Scientific Computing, 31 (2009), pp. 2549–2567, https://doi.org/10.1137/080727890.

[34] H. Zhang, S. Abhyankar, E. Constantinescu, and M. Anitescu, *Discrete adjoint sensitivity analysis of hybrid dynamical systems with switching*, IEEE Transactions on Circuits and Systems I: Regular Papers, 64 (2017), pp. 1247–1259, https://doi.org/10.1109/TCSI.2017.2651683.

[35] H. Zhang, R. T. Mills, K. Rupp, and B. F. Smith, *Vectorized parallel sparse matrix-vector multiplication in PETSc using AVX-512*, in Proceedings of the 47th International Conference on Parallel Processing - ICPP 2018, ACM Press, 2018, pp. 1–10, https://doi.org/10.1145/3225058.3225100.

[36] H. Zhang and A. Sandu, *FATODE: a library for forward, adjoint, and tangent linear integration of ODEs*, SIAM Journal on Scientific Computing, 36 (2014), pp. C504–C523, https://doi.org/10.1137/130912335.